Transactions of the Materials Research Society of Japan 30[1] 221-224 (2005)

Characterization of Amorphous Hafnium Silicate and Hafnium Aluminate Films by Grazing-Incidence X-ray Scattering

Ichiro Hirosawa, Hiroshi Kitajima,* and Kazuyoshi Torii*
Japan Synchrotron Radiation Research Institute, 1-1-1 Kouto, Mikazuki, Hyogo, Japan 679-5198
Fax: 81-791-58-1873, e-mail: hirosawa@spring8.or.jp
*Semiconductor Leading Edge Technologies. Inc. 16-1 Onogawa, Tsukuba, Ibaraki, Japan
Fax: 81-29-849-1186, e-mail: torii@selete.co.jp

We proposed grazing incidence X-ray diffraction to characterize hafnium-based insulating film. Radial distribution functions (RDFs) of hafnium silicate ($Hf_{0.6}Si_{0.4}O_x$) and hafnium aluminate ($Hf_{0.3}Al_{0.7}O_x$) films were derived from a grazing-incidence X-ray scattering experiment at BL46XU in SPring-8. In the RDF of $Hf_{0.6}Si_{0.4}O_x$ there were peaks at 0.214, 0.344, and 0.399 nm. The peak at 0.214 nm is attributed to oxygen atoms surrounding Hf, and the coordination number is similar to that of crystalline HfO_2. Coordination numbers of peaks at 0.344 and 0.399 nm are estimated to be 7.7 and 3.8 by assuming that these shells are composed of Hf and Si atoms. These estimated coordination numbers and interatomic distances are also very close to crystalline HfO_2; therefore we conclude that the structure of crystalline HfO_2 is preserved in the local structure of $Hf_{0.6}Si_{0.4}O_x$ film. On the other hand, only two peaks appear at 0.214 and 0.348 nm in the RDF of the aluminate film. Coordination numbers of these two peaks are very different from those of crystalline HfO_2.

Key words: hafnium silicate, hafnium aluminate, radial distribution function, grazing-incidence X-ray scattering

1. INTRODUCTION

To enable the scaling of complimentary metal-oxide-semiconductor (CMOS) technology to continue, many material systems has been studied as replacements for SiO_2[1]. Recently, many research groups have focused on hafnium-based systems and investigating their properties. In paticular, amorphous hafnium-silicate ($HfSiO_x(N)$) and hafnium-aluminate ($HfAlO_x$) have been paid much attention for poly-Si gate CMOS, because of their good transistor performances and thermal stability. However, their structures at the atomic scale have been unclear, since they are thin amorphous films on Si substrates.

In grazing-incidence X-ray scattering, the incident X-rays impinge on a sample surface with a very small incident angle [2]. Since the dielectric constant or refractive index of condensed matter is slightly less than unity, the incident X-rays are totally reflected at the surface if the incident angle is set below the critical angle. In this case, the penetration of X-rays is limited to several nanometers from the sample surface, and X-ray scattering from the substrate is drastically reduced. Thus, grazing-incidence X-ray scattering is a suitable technique for investigating a surface structure or a thin film structure on a substrate [3-7]. We examined the suitability of grazing–incidence X-ray scattering method for characterizing $Hf_{0.6}Si_{0.4}O_x$ and $Hf_{0.3}Al_{0.7}O_x$ films on Si substrates.

2. EXPERIMENT

Before the deposition of ALD-HfAlO or MOCVD-HfSiO film, thin SiON or SiO_2 layers were formed on Si substrates, respectively. The details of ALD-HfAlO/SiON/Si and MOCVD-HfSiO/SiO2/Si formation are described elsewhere [8-10].

X-ray reflectivity measurement was performed to determine the electron densities and film thicknesses of $Hf_{0.6}Si_{0.4}O_x$ and $Hf_{0.3}Al_{0.7}Ox$ films at BL19B2 in SPring-8. The energy of the incident beam was selected to be 9.4 keV using a Si(111) double-crystal monochromator. Two Rh-coated mirrors on the downstream side of the monochromator were used to reduce higher harmonics and to vertically focus the incident beam at the sample. An ion chamber monitored the intensity of the incident X-rays. The X-rays reflected from the sample were detected by an NaI scintillation counter in the scattering angle range from 0° to 2°.

Fig. 1.

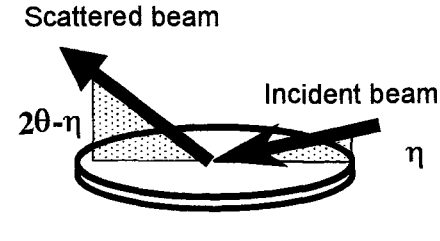

Grazing-incidence X-ray scattering experiments on $Hf_{0.6}Si_{0.4}O_x$ and $Hf_{0.3}Al_{0.7}O_x$ films were performed at BL46XU in SPring-8. The energy of the incident X-rays was set to 15.0 keV using the Si(111) double-crystal monochromator. Contamination from higher harmonics in the incident X-rays was reduced by two Pt-coated mirrors. The height and width of the incident beam were 0.05 and 1.00 mm, respectively. An ion chamber monitored the intensity of the incident X-rays. The

X-rays scattered from the sample were detected through a Soller slit by an NaI scintillation counter. The vertical and horizontal apertures of the receiving slit just behind the Soller slit were 10.0 mm and 2.0 mm, respectively. The detectors scanned from 2° to 150° in 0.5° steps in the vertical plane. The sample was mounted in a chamber filled with He gas to reduce the background intensity of scattering by air. The incident angle of X-rays to the sample surface was 0.1°. The scattering profile of the Si substrate from 2° to 122° was also observed in the same condition to estimate the background profile.

The powder diffraction pattern of crystalline HfO_2 (Kojundo Chemical Laboratory Co.) was also collected for reference using a Debye-Scherrer camera installed at BL19B2 in SPring-8. The energy of X-rays for the powder diffraction was 27.0 keV. HfO_2 powder was placed in a glass capillary tube with a diameter of 0.3mm. The diffraction pattern of the sample was recorded on an imaging plate.

3. RESULTS AND DISCUSSION

3.1 X-ray reflectivity

The observed X-ray reflectivities of $Hf_{0.6}Si_{0.4}O_x$ and $Hf_{0.3}Al_{0.7}O_x$ films are shown by the open circles in Fig. 2. The electron densities and film thicknesses of these two films were estimated by fitting. Electron densities of SiON or SiO_2 under-layers were set to 656.7 electrons/nm^3. In the case of $Hf_{0.6}Si_{0.4}O_x$, the observed reflectivity could be fitted by two separate layers of hafnium silicate. The thickness and electron density of the upper layer were estimated to be 28.36 nm and 1801.6 electrons/nm^3, respectively. Those of the lower layer were 12.20 nm and 1633.7 electrons/nm^3. On the other hand, the observed reflectivity of the $Hf_{0.3}Al_{0.7}O_x$ films could be fitted by a single hafnium aluminate layer 22.1 nm thick with 1569.3 electrons/nm^3. Other estimated parameters are listed in Table I and II. Reflectivities calculated using the estimated parameters are indicated by solid curves in Fig. 2.

Table I. Estimated parameters of $Hf_{0.6}Si_{0.4}O_x$

	Density (electron/nm^3)	Thickness (nm)	Roughness (nm)
$Hf_{0.6}Si_{0.4}O_x$	1801.6	28.36	0.8
$Hf_{0.6}Si_{0.4}O_x$	1633.7	12.20	11.4
SiO_2	656.7	1.67	1.0

Table II. Estimated parameters of $Hf_{0.3}Al_{0.7}O_x$

	Density (electron/nm^3)	Thickness (nm)	Roughness (nm)
$Hf_{0.3}Al_{0.7}O_x$	1569.3	22.1	0.5
SiO_2	656.7	1.65	0.5

3.2 Grazing-incidence X-ray scattering

When the incident angle was 0.1°, the penetration depths of X-rays into the $Hf_{0.6}Si_{0.4}O_x$ and $Hf_{0.3}Al_{0.7}Ox$ films were calculated to be about 3.5 nm from their electron densities. We conclude that the intensities detected in this experiment were X-rays scattered from the $Hf_{0.6}Si_{0.4}O_x$ and $Hf_{0.3}Al_{0.7}O_x$ films, because these films were thicker than the X-ray penetration depth. Detected intensity of the $Hf_{0.6}Si_{0.4}O_x$ film mainly came from its dense upper layer. As shown in Fig. 3, the lower intensity detected from the Si substrate also proved that the observed profile mainly came from the $Hf_{0.3}Al_{0.7}O_x$ films.

Fig. 2.

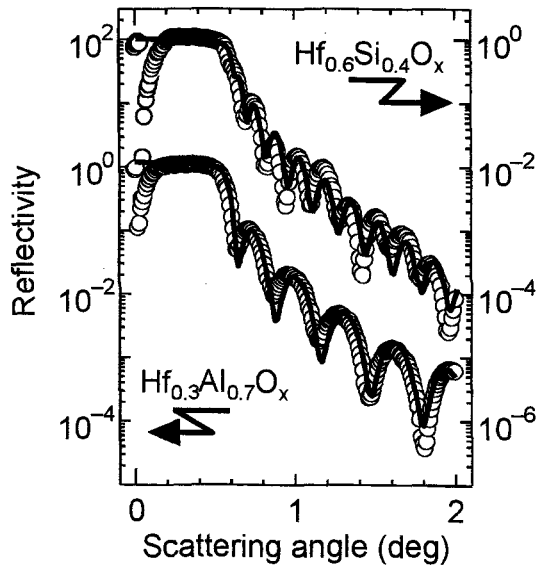

X-ray reflectivities of the $Hf_{0.6}Si_{0.4}O_x$ (right scale) and $Hf_{0.3}Al_{0.7}O_x$ (left scale). Open circles indicate observed data and solid curves are calculated ones using optimized parameters.

Fig. 3.

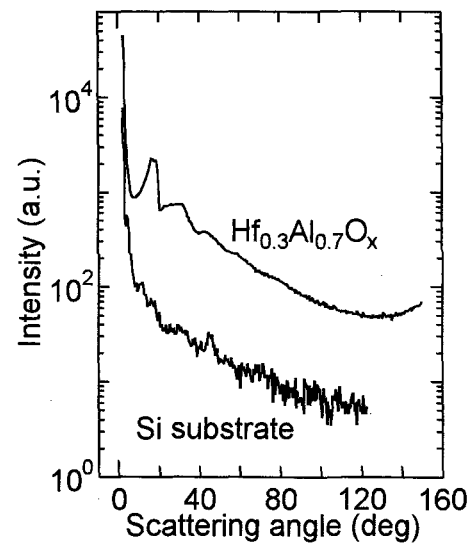

Observed profiles of $Hf_{0.3}Al_{0.7}O_x$ film and Si substrate. Intensities are normalized by monitor counts.

The observed intensities from the films decreased sharply as the scattering angle (2θ) changed from 2° to 6°. Below 6°, the detected intensity mainly came from the scattering by the He atmosphere around the sample, because nearly the same profile was also observed for the Si substrate, as shown in Fig. 3. In the small scattering angle region, the background intensity of the He atmosphere fitted well to the formula:

$$A\exp(-Bq)$$

where A and B are optimized parameters, and q is the wavenumber of the scattering vector ($=4\pi\sin\theta/\lambda$). Background profiles were approximated as third-order polynomials of q in the outer region from 9°. Thus, in the correction procedure to derive the interference function defined as $(I/N-\Sigma f_i^2)/\Sigma f_i^2$ (I/N: normalized intensity in electron units, f_i: atomic form factor) [11], the observed profiles were fitted with the following formula:

$$A\exp(-Bq)+c_0+c_1q+c_2q^2+c_3q^3+s\Sigma f_i^2$$

The tuned parameters for the fitting are A, B, c_0, c_1, c_2, c_3, and s in the above formula [6,7].

The effect of the polarization factor was neglected in the correction procedure because the incident X-rays were linearly polarized in the horizontal direction. Only geometrical correction was performed. For grazing-incidence X-ray scattering with incident angle η, the footprint of the incident X-rays spread to 1/sin η times the vertical size of the incident beam on the sample surface. On the other hand, the portion of detected X-rays from the sample surface was determined by the projection of the Soller slit aperture on the sample surface. Thus, the portion of detected intensity depends on the scattering angle, the X-ray footprint, and vertical aperture of the Soller slit. The expression of the geometrical correction factor G is $H_r/\sin(2\theta-\eta)$ in the 2θ region from η+ arc $\sin((H_d \sin\eta)/H_r)$ to < π/2+η+ arc $\sin((H_d \sin\eta)/H_r)$, where H_d and H_r are the vertical apertures of the divergence and receiving slits. Otherwise, G is defined as $H_d/\sin\eta$ [6,7]. There is no need for geometrical correction to derive the interference function of the bulk HfO_2.

Oscillations of the wavenumber-weighted interference functions (q-weighted interference functions) of the $Hf_{0.6}Si_{0.4}O_x$ and $Hf_{0.3}Al_{0.7}O_x$ films and HfO_2 powder were clearly seen to 120 nm^{-1}, as shown in Fig. 4.

3.3 Radial distribution function

The Fourier transform of the interference functions of the $Hf_{0.6}Si_{0.4}O_x$ and $Hf_{0.3}Al_{0.7}O_x$ films in the range of 4.0–14.1 nm^{-1} yields radial distribution functions with

$$4\pi\rho r^2 + 2r/\pi\int q(I/N-\Sigma f_i^2)\sin(qr)/\Sigma f_i^2\,dq,$$

where r and ρ are the distance and averaged electron densities listed in Table I or II [6,7]. The radial distribution function of the HfO_2 powder was also derived by Fourier-transformation in the range of 0.1–16.8 nm^{-1}. The averaged electron density of HfO_2 was estimated to be 2545.0 electrons/nm^3 from the crystal structure data of monoclinic HfO_2 [12]. Positions and areas of peaks in radial distribution functions inform interatomic distances and coordination numbers. In this discussion, positions and areas of peaks were determined by fitting with Gaussian functions.

The radial distribution function of HfO_2 derived from its powder diffraction pattern has clear peaks at 0.217 nm (A), 0.346 nm (B), and 0.396 nm (C) as shown in Fig. 5. The peak at 0.217 nm (A) is considered to be the pair correlation Hf-O. Its coordination number estimated

Fig. 4.

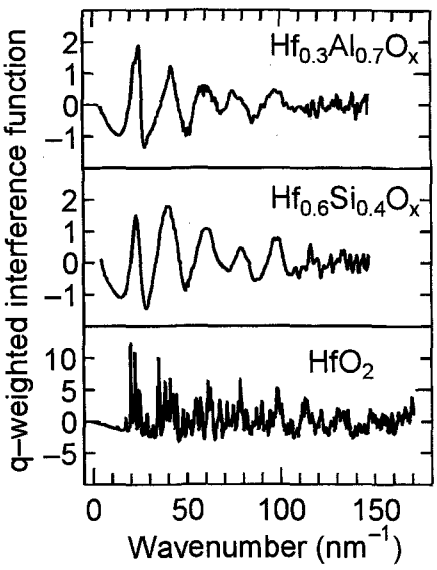

Wavenumber-weighted interference functions (q-weighted interference functions) of hafnium silicate and aluminate films, and bulk HfO_2 from their observed profiles.

Fig. 5.

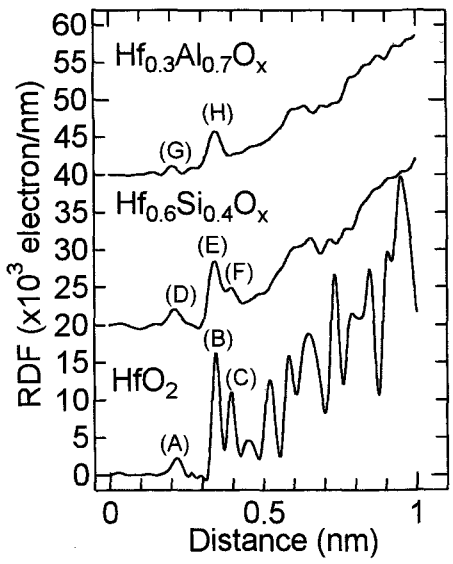

Radial distribution functions of $Hf_{0.3}Al_{0.6}O_x$, $Hf_{0.6}Si_{0.4}O_x$ films, and crystalline bulk HfO_2.

by area integration of the peak is consistent with the crystal structure of monoclinic HfO_2 [12]. The peaks at 0.346 nm (B) and 0.396 nm (C) mainly come from the first and second Hf-Hf shells, respectively. These two peaks can also be precisely explained by the crystalline monoclinic HfO_2 [12], and the areas of these peaks are consistent with their coordination numbers of 7 and 4. However, O-O correlation around 0.28 nm is not seen in this radial distribution function for smaller scattering amplitudes of the oxygen atom.

The derived radial distribution function of the $Hf_{0.6}Si_{0.4}O_x$ film also has peaks at 0.214 nm (D), 0.344nm (E), and 0.399 nm (F), which strongly suggests that the number of oxygen atoms surrounding hafnium in the $Hf_{0.6}Si_{0.4}O_x$ film was nearly the same as that in bulk HfO_2, because the area of the peak at 0.214 nm (D) of $Hf_{0.6}Si_{0.4}O_x$ is nearly the same as that of the peak at 0.217 nm (A) of the bulk HfO_2. On the other hand, the peaks at 0.344 nm (E) and 0.399 nm (F) of the $Hf_{0.6}Si_{0.4}O_x$ film are considerably lower than the two corresponding peaks (B and C) of the crystalline HfO_2. However, assuming that 40% of hafnium atoms were randomly replaced by silicon atoms, the coordination numbers were estimated to be 7.7 and 3.8 for the peaks at 0.344 nm (E) and 0.399 nm (F), respectively. Thus, the local structure around hafnium in the $Hf_{0.6}Si_{0.4}O_x$ film is close to that of monoclinic HfO_2.

The radial distribution function of the $Hf_{0.3}Al_{0.7}O_x$ film has only two peaks: one at 0.214 nm (G) and the other at 0.348 nm (H). There are no peaks corresponding to the second shell of Hf-Hf correlation seen in the radial distribution functions of crystalline HfO_2 and $Hf_{0.6}Si_{0.4}O_x$ film. One might consider that the peak at 0.214 nm (G) corresponds to Hf-O correlation, but its coordination number was much lower than that of the monoclinic HfO_2. As for the peak at 0.348 nm (H), the coordination number was estimated to be 12.8 by assuming that 70% of hafnium atoms were randomly replaced by aluminum atoms. This value is considerably higher than for the first Hf-Hf shell of the crystalline HfO_2. These characteristics of the $Hf_{0.3}Al_{0.7}O_x$ film indicate that the features of crystalline HfO_2 were reduced in the $Hf_{0.3}Al_{0.7}O_x$ film.

Fig.6

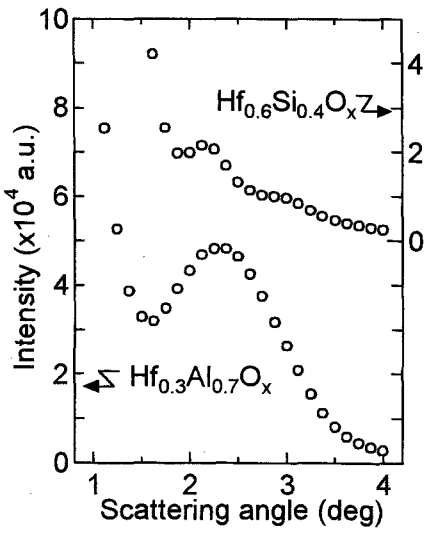

Profiles of first sharp diffraction peaks in hafnium silicate (right scale) and hafnium aluminate (left scale) films.

3.4 First sharp diffraction peaks

The first sharp diffraction peaks were observed in the $Hf_{0.6}Si_{0.4}O_x$ and $Hf_{0.3}Al_{0.7}O_x$ films, as shown in Fig. 6. These are signatures of intermediate range ordering [13]. The correlation lengths were estimated to be 2.2 and 2.0 nm for the $Hf_{0.6}Si_{0.4}O_x$ and $Hf_{0.3}Al_{0.7}O_x$ films, respectively [13].

4. SUMMARY

We applied the grazing-incidence X-ray scattering method to characterize the amorphous $Hf_{0.6}Si_{0.4}O_x$ and $Hf_{0.3}Al_{0.7}O_x$ films on silicon substrates. We clarified that the crystalline HfO_2 structure was preserved in the amorphous $Hf_{0.6}Si_{0.4}O_x$ film by comparing their radial structural functions derived from observed X-ray scattering profiles. By assuming that hafnium atoms were randomly replaced by silicon atoms in amorphous $Hf_{0.6}Si_{0.4}O_x$ film, we found that the interatomic distances and coordination numbers of the first, second, and third shells from the hafnium atom in amorphous $Hf_{0.6}Si_{0.4}O_x$ film were close to those of crystalline HfO_2. On the other hand, the local structure around hafnium in the $Hf_{0.3}Al_{0.7}O_x$ film was considerably different from that of crystalline HfO_2. We also detected intermediate range ordering in both films. Thus, we conclude that grazing-incidence X-ray scattering is applicable for characterizing hafnium-based insulating film.

REFERENCES

[1] G. D. Wilk, R. M. Wallance, and J. M. Anthony, *J. Appl. Phys.* **89**, 5243-5273 (2001).
[2] W. C. Marra, P. Eisenberger, and A. Y. Cho, *J. Appl. Phys.* **50**, 6927-6933 (1979).
[3] I. Hirosawa, A. Akimoto, T. Tatsumi, J. Mizuki, and J. Matsui, *J. Cryst Growth.* **103**, 150-155 (1990).
[4] B. J. Factor, T. P. Russell, and M. F. Toney, *Phys. Rev. Lett.* **66**, 1181-1184 (1991).
[5] I. Hirosawa, N. Sasaki, and H.Kimura, *Jpn. J. Appl. Phys.* **38**, L583-L585 (1999).
[6] I. Hirosawa, Y. Uehara, M. Sato and N. Umesaki, *J. Ceramic Soc. Jpn.* **112-1**, S1476-S1478 (2004).
[7] M.Sato, T.Matsunaga, T. Kouzaki, and N. Yamada, *Mat. Res. Soc. Symp. Proc.* **803**, 245-250 (2004).
[8] T. Kawahara, K. Torii, R. Mitsuhashi, A. Mutoh, A. Horiuchi, H. Ito, and H. Kitajima, *Ext. Abstr. IWGI2003*, 23-24 (2003).
[9] R. Mitsuhashi, A. Horiuchi, A. Uedono, and K. Torii, *Ext. Abstr. IWGI2003*, 150-151 (2003).
[10] T. Aoyama, S. Kamiyama, Y. Tamura, T. Sasaki, R. Mitsuhashi, K. Torii, H. Kitajima, and T. Arikado, *Ext. Abstr. IWGI2003*, 174-176 (2003).
[11] H. F. Poulsen, J. Neuefeind, H. B. Neumann, J. R. Schneider, and M. D. Zeidler, *J. Non.-Cryst. Solids.* **188**, 63-74 (1995).
[12] R. Ruh and P. W. R. Corfield, *J. Am. Ceramic Soc.* **53**, 126-129 (1970).
[13] J. Swenson and L. Borjesson, *J. Non-Cyst. Solids* **223**, 223-229 (1998).

(Received January 7, 2005; Accepted February 1, 2005)